Sensors & Transducers, Vol. 210, Issue 3, March 2017, pp. 9-16

www.sensorsportal.com

Sensors & Transducers

Published by IFSA Publishing, S. L., 2017
http://www.sensorsportal.com

Development of Perovskite Sensitized Thin Film Solar Cells Based on Graphene Oxide/TiO_2 Photoanodes

[1] Momina KHANNAM, [1] Shyamalima SHARMA, [2] Ranoo BHARGAV, [2] Asit PATRA and [1, *] Swapan Kumar DOLUI

[1] Department of Chemical Sciences, Tezpur University, Napaam, Tezpur, Dist. Sonitpur, Assam-784028, India

[2] Physics of Energy Harvesting Division, CSIR-National Physical Laboratory, Dr. K. S. Krishnan Road, Pusa, New Delhi-110 012, India

[*] Tel.: 9957198489

[*] E-mail: dolui@tezu.ernet.in

Received: 9 January 2017 /Accepted: 3 March 2017 /Published: 31 March 2017

Abstract: Graphene oxide/TiO_2(GO/TiO_2) nanocomposites with different concentrations of GO were prepared by a self-assemble method. The synthesized GO/TiO_2 nanocomposites are characterized by X-ray diffraction (XRD), scanning electron microscopy (SEM), and transmission electron microscopic (TEM) analysis. Using these GO/TiO_2 nanocomposites as an electron collection layer a series of solid state perovskite sensitized solar cells were fabricated. The photovoltaic properties like short circuit current density and photo conversion efficiency of the fabricated device were evaluated. It was noticed that the nanocomposites has significant effects on the photovoltaic properties of the device. With increase in the amount of GO in the nanocomposites the short circuit current density of the devices increased from 1.79 to 4.65 $mAcm^{-2}$ and the photo conversion efficiency increased from 0.413 to 1.34 %.

Keywords: Nanocomposites, Perovskite, Solar cells, Graphene oxide, PCE.

1. Introduction

Now a days, the growing energy demand can be fulfilled to a large extent by utilizing a small fraction of solar radiation. Different solar cells such as amorphous and nanocrystalline Si [1], inorganic compound semiconductors [2], quantum dot solar cells (QDSCs) [3], dye-sensitized solar cells (DSSCs) [4], organic solar cells (OSCs) [5] and now perovskite-based meso-superstructured solar cells (MSSCs) [6] have been developed to achieve the needs. Evolving from liquid electrolyte based DSSCs, solid-state perovskite-based solar cells, made by using methylammonium lead iodide ($CH_3NH_3PbI_3$) perovskite materials coated upon the surface of mesoscopic TiO_2 substrates, have shown a very promising efficiency. Organo-metal halide perovskites with low loss in photovoltaic operation have been employed as the absorber layer in hybrid solar cells. The organo-metal can be synthesized by a simple solution based synthetic route from abundant sources like C, N, Pb, and halogens [7]. With large absorption coefficient [8], higher carrier mobility [9], and direct band gap lead halide inorganic layer is an attractive class of materials as light harvesters in heterojunction solar cells.

For the first time Miyasaka and co-workers reported a methylammonium lead iodide "perovskite sensitized" solar cell by employing a liquid electrolyte in a conventional dye-sensitized solar cell (DSSC) architecture which gives an efficiency of 3.8 % [10]. Perovskite can be used also as an efficient light harvester as well as a HTM in the fabricated devices. However, to get a better efficiency, HTM is used

which collects the holes and transfers them to the back electrode. Solar cells employing methylammonium lead iodide perovskite absorber materials on mesoscopic TiO_2 have shown very promising efficiency. The conduction and valence band of the methylammonium lead iodide injects electron into the TiO_2 and whole transport to the back contact respectively. Now a days, a wide variety of organic polymer hole-conductors are used in these perovskite solar cells [11-13]. The most outstanding among these hole-conducting polymers is spiro-OMeTAD (2,2′,7,7′-tetrakis(N,N-di-p-methoxy phenylamine)-9,9′-spirobifluorene) which gives a very high PCE of 9.7 % as reported by Kim and his co-workers [14].

In many growing technologies, TiO_2 has drawn special attention with the advantage that it can prevent shunting and leakage currents under reverse bias [15]. In general, TiO_2 coated conductive substrate is used as an electron collection layer which plays a very important role in thin-film solar cells by facilitating selective charge collection. However, these materials have some major drawback as it requires high-temperature processing to increase their crystallinity and charge carrier mobility [16].

In the meantime, the two dimensional material graphene have got numerous fundamental development with a number of unique properties. Graphene is identified as one of the strongest materials with very high thermal and electrical conductivity [17]. In addition, graphene possesses high charge mobility [18-19] as well as high optical transmittance [20-21]. With these unique properties of graphene, it find diverse field applications like photovoltaics, photocatalysis, nanoelectronics, sensors, etc. [22-24]. With the introduction of graphene in TiO_2 based nanocomposites, the strong interfacial interaction among the components facilitated the high conductivity and better electrical properties of such materials [25-27].

Inspired from the foregoing discussion, we have developed a series of nanocomposites based on graphene oxide (GO) and nano TiO_2. The synthesized GO/TiO_2 then employed as the electron selective contact to fabricate organo metal halide perovskite solar cell. The photovoltaic properties like short circuit current density and the photo conversion efficiency of the fabricated device were evaluated as a function of GO content.

2. Experimental Section

2.1. Reagents

Sodium nitrate ($NaNO_3$), potassium permanganate ($KMnO_4$), sodium dodecyl sulfate ($CH_3(CH_2)_{11}OSO_3Na$) (Merck), $TiCl_3$ (Merck), Sodium sulfate (Na_2SO_4), Hydrogen peroxide (H_2O_2) were purchased from Merck India.Methylamine (aqueous, 40 %), hydroiodic acid (aqueous, 57 %), ITO-coated glass, PbI_2&DMF, P3HT, Graphite powder were purchased from Sigma Aldrich India.

2.2. Synthesis of GO/TiO_2 Nanocomposites

2.2.1. Synthesis of Graphene Oxide

Graphene oxide was synthesized from natural graphite by using Hummers method [28]. Briefly, the method is graphite (5 g), $NaNO_3$ (2.5 g) and H_2SO_4 (120 mL) were mixed in a 500 mL beaker and the mixture was stirred vigorously in an ice bath for 30 min. Under constant stirring 15 g of $KMnO_4$ was added to the above suspension in a very controlled way so that the reaction temperature remains below 20 °C The mixture was kept under stirring for 12 h at room temperature, followed by the addition of 150 mL of distilled water and kept for 24 h under constant stirring. Then 50 mL of 30 % H_2O_2 was added to the mixture and stirred for another 6 h. Finally, the obtained product was washed with 5 % HCl and followed by distilled water so that the pH of the filtrate becomes 7 and dried in vacuum oven. The obtained graphene oxide was then dispersed and exfoliated in deionized water by using an ultrasonic bath for 40 min. The obtained graphene oxide suspension was then used for the synthesis of GO/TiO_2 composites.

2.2.2. Synthesis of Graphene Oxide/TiO_2 Composites

GO/TiO_2 composites were synthesized by a previously reported self-assembly method [29]. The graphene oxide suspension (1.3 gL^{-1}) as obtained was diluted with water and sodium dodecyl sulfate was added. To this mixture an aqueous solution of $TiCl_3$ (0.12 mol L^{-1}) was added and kept for 1 h under constant stirring. To the mixture, 10 ml of 0.6 M Na_2SO_4 solution and 5 mL of 1 wt % H_2O_2 solution was added and continued stirring for another 1 h at 90 °C. The final precipitates of the reactions were separated and washed with water and ethanol and then dried at 70 °C. Finally, the dried product was calcinated at 400°C for 2 h. Four sets of GO/TiO_2 nanocomposites viz. GO/TiO_2-A, GO/TiO_2-B, GO/TiO_2-C & GO/TiO_2-D having GO wt% of 0.25, 0.5, 1 & 2.5 respectively were synthesized by taking different amounts of graphene oxide, water and sodium dodecyl sulfate accordingly. The compositions of the prepared GO/TiO_2 nanocomposites are given in Table 1.

Table 1. The compositions of the prepared GO/TiO_2 nanocomposites.

TiO_2	GOTiO_2-A (0.25 wt%)	GOTiO_2-B (0.5 wt%)	GOTiO_2-C (1 wt%)	GOTiO_2-D (2.5 wt%)
GO (ml)	1.85	3.7	7.4	18.5
SDS (ml)	0.11	0.22	0.44	1.1

2.3. Synthesis of Methylammonium Iodide

Methylammonium iodide was synthesized by reacting 10 mL of methylamine (40 %, aqueous) and 10.8 mL of hydroiodic acid (57 %, aqueous) in a round bottom flask under constant stirring at 0 °C for 2 h. The product of the reaction was recovered by evaporating the solvents at 50 °C in a rotary evaporator. The obtained yellowish product was then washed three times with diethyl ether and dried. The whitish solid was collected and dried in a vacuum oven at 60 °C for 24 h [30].

2.4. Fabrication of the Perovskite Based Solar Cells

The ITO-coated glass substrate was cleaned before fabrication by ultrasonicating in detergent and deionized water followed by treating with boiled acetone and isopropanol and dried in air. There after a thin compact blocking layer of GO/TiO_2 composites were spin coated (2000 rpm for 60 seconds) onto the ITO film followed by annealed at 200 °C for 60 minutes. The synthesis of methylammonium lead iodide on the TiO_2 composite layer was carried out by spin coating the precursor solution at 2000 rpm for 60 seconds, which was prepared by dissolving the equimolecular mixture of CH_3NH_3I and PbI_2 in DMF under glove box conditions. Then the film was annealed at 100 °C for 45 minutes in a hotplate. The change of color of the film upon drying confirms the formation of methylammonium lead iodide. The P3HT layer was then spin coated by employing the P3HT/Chlorobenzene solution (20 mg mL^{-1}) at 1500 rpm for 45 seconds. Finally, the fabrication was completed by the counter electrode deposition on the prepared film by thermal evaporation of aluminium at a pressure of 2×10^{-5} Pa. The active area of the fabricated solar cells was assessed and found to be 0.04 cm^2. The photovoltaic characteristics of the fabricated solar cells were evaluated with the help of a Keithley SourceMeter and under illumination with a simulated (AM 1.5) solar light at 1 sun (100 mW cm^{-2}).

2.5. Measurements

2.5.1. X-ray Diffractometer (XRD)

The XRD measurements were carried out in a Rigaku X-ray diffractometer (Miniflex, UK) using CuKα (λ=0.154 nm) radiation at a scanning rate of 2° min^{-1} with an angle (2θ) ranging from 10° to 80° to study the structural characteristics of the synthesized nanocomposites.

2.5.2. Ultraviolet-visible (UV-vis) Spectroscopy

The optical property of MWCNT@TiO_2 nanocomposites were measured by using UV-Visible diffuse reflectance spectra in the range 200–800 nm using Shimadzu UV-2550 UV–visible spectrophotometer.

2.5.3. Scanning Electron Microscopy (SEM)

The surface morphologies of the prepared samples were studied by using a Jeol-JSM-6390L V scanning electron microscope at an accelerating voltage of 5-15 kV. The surface of the samples was Pt-coated before the scanning.

2.5.4. Transmission Electron Microscopy (TEM)

To study the distribution of the of particles within the nanocomposites, TEM analysis was done in a JEOL, JEM 2100 transmission electron microscope at an accelerating voltage of 200 kV.

2.6. Photovoltaic Test

The photocurrent voltage characteristics curves of the fabricated gel electrolyte based DSSCs were carried out using a 100 mW cm^{-2} xenon arc lamp in ambient atmosphere. The performance parameters of the fabricated devices i.e. the cell fill factor (FF) and cell power conversion efficiency (Η) were calculated by following Eqn. (1) and Eqn. (2) respectively.

$$FF = \frac{J_{max} \times V_{max}}{J_{sc} \times V_{oc}}, \quad (1)$$

$$\eta(\%) = \frac{FF \times J_{sc} \times V_{oc}}{P_{in}} \times 100, \quad (2)$$

where V_{max} and J_{max} are the maximum current density and voltage respectively at the point of maximum power of the photocurrent density versus voltage plot. J_{sc} is the short circuit current density (mA cm^{-2}), V_{oc} is the open circuit voltage (V) and P_{in} is the intensity of the incident white light.

3. Results and Discussions

3.1. UV-Visible Analysis

To study the optical property of the prepared GO/TiO_2 nanocomposites, UV-Visible analysis was recorded in the range of 200-800 nm and the spectra are shown in Fig. 1(a).

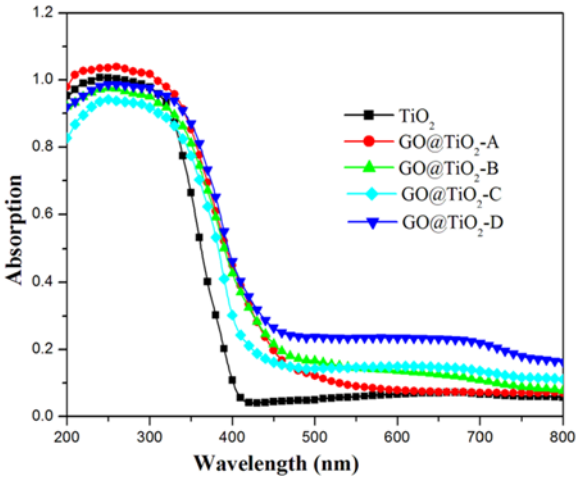

Fig. 1(a). UV-vis absorption spectra for TiO_2 and GO@TiO_2 nanocomposites.

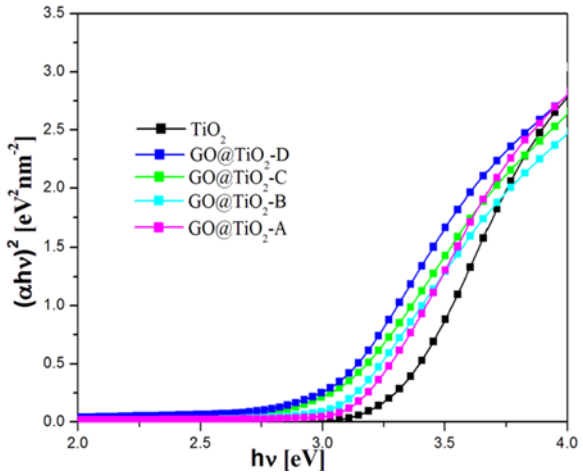

Fig. 1(b). Tauc's plot for optical band-gap calculation for TiO_2 and GO@TiO_2 nanocomposites.

All the nanocomposites shows the same absorption profile with a steep absorption edge at around 400 nm which are in the UV region of electromagnetic radiation which is caused by the bonding effect between GO and TiO_2. This kind of typical absorption in the UV region can be attributed to the intrinsic band gap absorption of TiO_2 resulting from the electron transition from the valance band to the conduction band of TiO_2 [31]. The presence of different amounts of GO in the nanocomposites significantly influences the optical properties of the material. The light absorption intensity for the GO/TiO_2 nanocomposites is observed to be increased with increasing GO content. In addition, a peak broadening is also noticed with increasing GO content.

Optical band gap calculations are carried out using the Tauc's relationship. The Tauc's equation for band gap calculations is described as,

$$(\alpha h\upsilon)^{1/n} = C(h\upsilon - E_g), \qquad (3)$$

where α is the absorption coefficient of the solid at a certain value of wavelength λ, h is the Planck's constant, C is the proportionality constant, υ is the frequency of light, E_g is the band gap energy and n=1/2 for direct allowed band gap. Fig. 1(b) shows the relationship of (αhυ)1/2 vs photon energy (hυ=1239/λ) for TiO_2 and also the GO/TiO_2 nanocomposites.

It shows that the band gap for the bare TiO_2 is 3.20 eV, whereas the band gaps for GO/TiO_2 nanocomposites are 3.06, 3.0, 2.89 & 2.84 eV corresponding to GO/TiO_2-A, GO/TiO_2-B, GO/TiO_2-C & GO/TiO_2-D respectively. This result in turn supports the qualitative observation of a red shift in the absorption edge of GO/TiO_2 nanocomposites as compared to the bare TiO_2. There is a possibility that some of the unpaired π electrons of GO can bonded with the free electrons present on the surface of TiO_2 nanoparticles to form Ti-O-C structure, resulting in the shifting of valence band and reduction in the band gap [32].

3.2. Powder X-ray Diffractometer (XRD)

The X-ray diffraction patterns for the GO and the GO/TiO_2 composites with different weight % of TiO_2 are shown in Fig. 2.

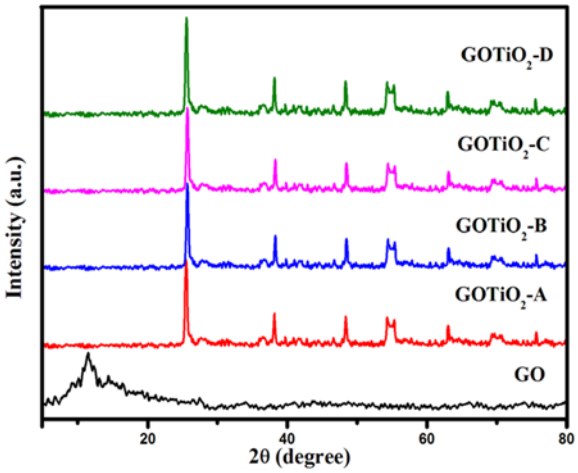

Fig. 2. XRD patterns of GO, GOTiO2-A, GOTiO2-B, GOTiO2-C & GOTiO2-D.

The neat GO exhibits a broad scattering peak at 2θ value of 11.5° corresponding to the plane (001) with an interlayer spacing of 7.43 Å [33]. The observed XRD patterns of the GO/TiO_2-A, GO/TiO_2-B, GO/TiO_2-C & GO/TiO_2-D represents the pure anatase phase of TiO_2 which is in turn confirmed by the reported JCPDs [34]. The reflection of (001) diffraction plane of GO is not observed in the XRD pattern of GO/TiO_2 composites which can be attributed to the fact that the regular stack of GO is disturbed by the intercalation of anatase TiO_2 [39, 41].

Thus, the XRD pattern of the GO/TiO_2 composites confirms the homogeneous distribution of anatse TiO_2

within the GO stacks. Furthermore, the existence of grapheme oxide in GO/TiO_2 nanocomposites can be clearly elucidated by Raman analysis.

3.3. Raman Spectra

Raman spectroscopy is a powerful tool to analyze the crystalline quality of the carbon and the defect mediated peaks. Fig. 3 shows the Raman spectrum of GO (inset graph in Fig. 3) and GO/TiO_2 nanocomposite. In the Raman spectrum first order dominant vibrational modes, D band 1351 cm^{-1} corresponds to the A1g symmetry mode of sp3 carbon indicates about the order or disorder in the system [34] and G band 1599 cm^{-1} corresponds to the vibrational mode of sp2 carbon provides information about the doubly degenerate E2g mode of the Brillonium zone centre [35].

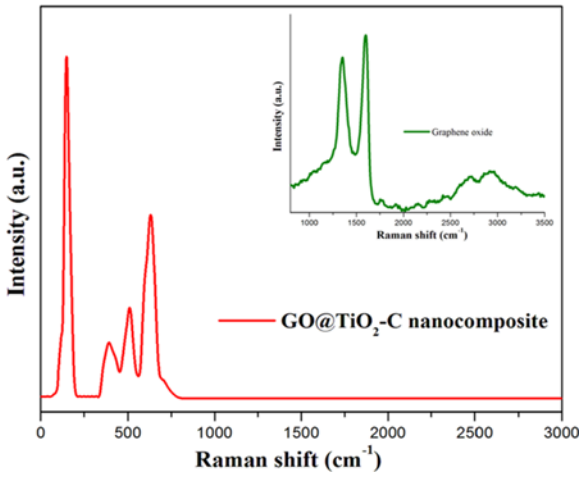

Fig. 3. Raman Spectra for GO and GO@TiO_2-C nanocomposite.

The second order vibrational bands, 2D1 & 2D2 arises at 2717.36 cm^{-1} & 2928.62 cm^{-1} respectively originates from a two phonon double resonance Raman process and provides information on the stacking order of graphene with no of layers and shows often a doublet with increasing no of graphene layers.

Another overtone weak band 2D/ is observed at 3194.23 cm^{-1} [36]. The intensity of G band is stronger than D band. In plane crystallite size, La can be calculated from the intensity ratio of the G band to the D band by using the formula, La= 4.4 (LG/LD). The obtained La value is 4.89, [38] from this it can be concluded that the sample contains highly disordered and randomly arranged graphene sheets. The shape of the 2D band is sensitive to the no of layers of graphene and chemical doping. When GO combines with TiO_2, the crystal structure of carbon changes obviously. There are four specific vibration modes are located at around 141 (E(g1)), 391 (B1g(1)), 514 (A1g+B1g(2)) & 634 cm^{-1} (Eg(2)) indicating the presence of the anatase phase of TiO_2 in the sample [39].

3.4. The Morphological Study of the Samples

3.4.1. SEM Analysis & EDX

The surface characteristics of the GO and the GO/TiO_2 nanocomposites are investigated with SEM analysis and the micrographs are shown in Fig. 4. For the pure GO a flat multilayered structure with stacked GO sheets is observed at higher magnifications (Fig. 4(a)) [40]. After introducing TiO_2 into the GO sheets (Fig. 4(c)), the SEM micrograph shows that the flat layered structure of the GO is disappeared and a rough surface morphology of the GO/TiO_2 nanocomposites is noticed. The change in the morphology of the GO/TiO_2 nanocomposites from the pure GO can be attributed to the successful incorporation of TiO_2 into the GO sheets. The energy dispersive X-ray spectrum (EDX) of the GO sheets and GO/TiO_2 nanocomposites indicates the successful distribution of TiO_2 nanoparticles into the GO sheets (Fig. 4(b) and Fig. 4(d)). The introduction of TiO_2 into the GO is confirmed from the elemental typical mapping images of titanium, oxygen and carbon.

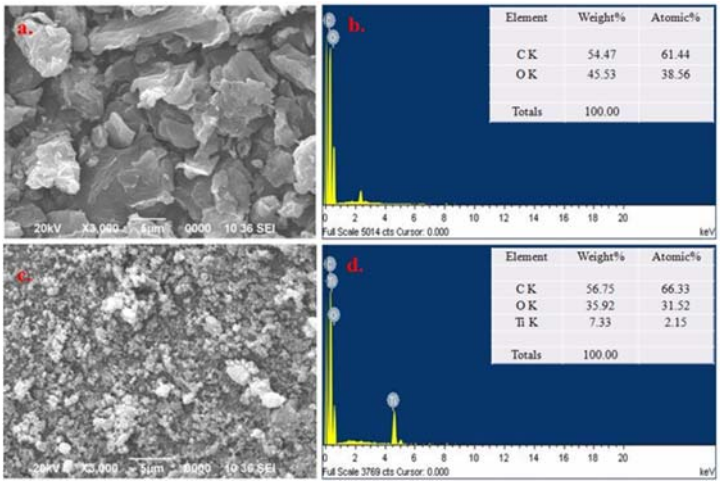

Fig. 4. SEM images & of EDX-spectrum of the GO (a & b) and GO@TiO_2-D nanocomposite (c & d).

3.4.2. TEM Analysis

The TEM micrographs of pure GO and GO/TiO_2 nanocomposites (GOTiO_2-D) are shown in Fig. 5. Layered and flake like structure with some wrinkles are observed in TEM micrographs of pure GO (Fig. 5(a)). The TEM micrographs of GO at high magnification (Fig. 5(b)) shows a completely amorphous and disordered structure [41]. A well dispersed TiO_2 nanoparticles on the surface of GO sheets are observed form the TEM micrographs of the nanocomposites Fig. 5(c & d). Moreover, the TiO_2 nanoparticles are homogeneously and closely dispersed on the GO sheets and thereby facilitate the electron transfer process in the solar cells.

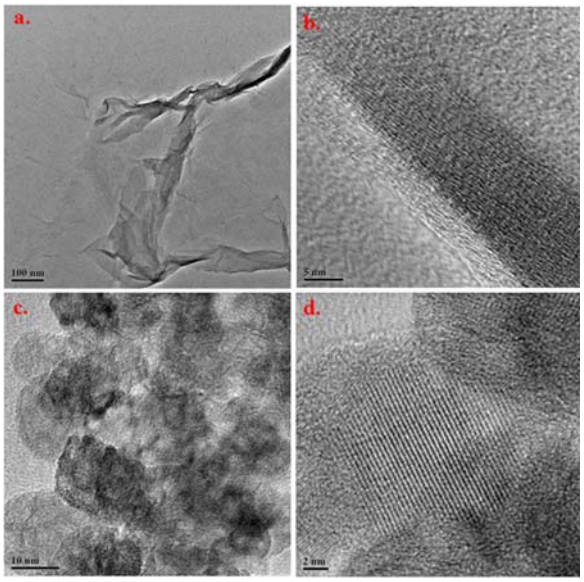

Fig. 5. TEM micrographs of the GO (a & b) and GO@TiO_2-D nanocomposite (c & d).

3.5. Photovoltaic Performance of the Fabricated Devices

Photovoltaic properties of the fabricated perovskite sensitized solar cells are examined by using different GO/TiO_2 composites having the device structure ITO/GO/TiO_2 nanocomposite/$CH_3NH_3PbI_3$/P3HT/Al. The photovoltaic performance parameters are summarized in Table 2 and the J-V curves are shown in Fig. 6.

Table 2. Device parameters of the GO/TiO_2 nanocomposite based solid state perovskite sensitized solar cells.

Sample	Jsc (mA cm^{-2})	Voc (V)	FF	PCE, η (%)
TiO_2 only	0.775	0.3656	0.426	0.121
GOTiO_2-A	1.785	0.453	0.496	0.401
GOTiO_2-B	2.771	0.505	0.434	0.608
GOTiO_2-C	3.812	0.507	0.546	1.055
GOTiO_2-D	5.286	0.5326	0.501	1.42

Here we investigate the performance of perovskite sensitized solar cells using different concentrations of GO in the TiO_2 nanocomposite which acts as the n-type charge collection electrode.

The mean solar cell performance parameters of the fabricated devices were measured under stimulated 100 mW cm^{-2} sunlight. We observed that, there is a clear enhancement in the device parameter of the fabricated devices by the introduction of GO in the TiO_2. By using the TiO_2 nanoparticles the short circuit current density (J_{sc}) and fill factor are found to be 0.81 mA cm^{-2} and 0.30 respectively. With increasing GO concentration in the electron collection layer both the Jsc and FF increases upto 4.65 mA cm^{-2} and 0.56 respectively.

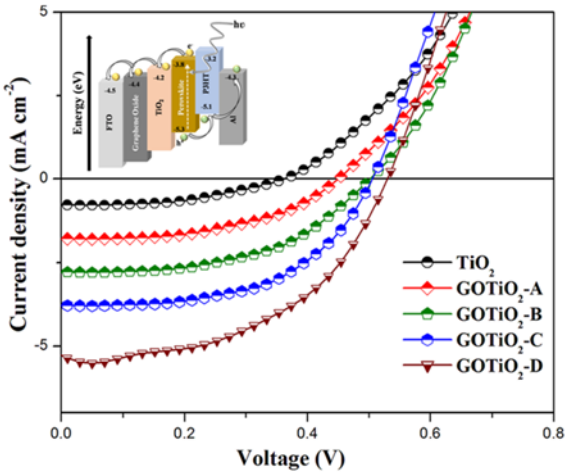

Fig. 6. Photocurrent density versus voltage plot of TiO_2, GOTiO_2-A, GOTiO_2-B, GOTiO_2-C & GOTiO_2-D.

Enhancement in the efficiency of the devices with the incorporation of the GO into TiO_2 can be described from the facts that GO has a work function that lies in-between that of the ITO and the conduction band of TiO_2. As a result of which GO containing TiO_2 acts as a better electron collector as compared to TiO_2 alone by reducing the energy barrier at the material interfaces and also due to the superior charge mobility of GO. In this device structure the organometal halide perovskite, methylammonium lead iodide acts as the absorber, coated upon the electron collection layer. While the interdigitated P3HT collects the holes and transfers them to the back electrode.

4. Conclusions

This work successfully demonstrates the application of two different combinations of graphene oxide with organo metal halide perovskite. Also the study of the synthesized GO/TiO_2 nanocomposites showed that with increase in the GO content there occurs enhancement in the optical properties. The homogeneous distribution of TiO_2 nanoparticles

within the GO stacks is confirmed by the XRD analysis, which can be further confirmed from the SEM and TEM micrographs that TiO_2 nanoparticles are homogeneously and closely dispersed on the GO sheets. The purpose of using GO/TiO_2 nanocomposites in perovskite sensitized solar cells is also beneficial as it behaves well as the electron collection layer. As a result of which there is a significant enhancement in the photovoltaic parameters of the solar cells. It has also been spotted form the study that the incorporation of high concentration of GO in the nanocomposite results in the enhancement of the device parameters i.e. VOC, JSC and PCE due to the superior charge mobility of GO.

Acknowledgements

The authors would like to acknowledge University Grant Commission (UGC), India, for providing Junior Research Fellowship (JRF) under Maulana Azad National Fellowship (MANF) scheme for financial assistance and Department of Electronics and Information Technology, Ministry of Communications & Information Technology India for their financial support (Sanction No. 1 (11)/2012-EMCD dated 05-03-2013). Authors are also very much grateful to SAIF, North-Eastern Hill University, India and SAIC, Tezpur University, India for analytical support.

References

[1]. M. A. Green, K. Emery, Y. Hishikawa, W. Warta, E. D. Dunlop, Solar cell efficiency tables (version 41), *Progress in Photovoltaics: Research and Applications,* Vol. 21, Issue 1, 2013, pp. 1-11.

[2]. P. Jackson, D. Hariskos, E. Lotter, S. Paetel, R. Wuerz, R. Menner, W. Wischmann, M. Powalla, New world record efficiency for Cu(In,Ga)Se_2 thin-film solar cells beyond 20 %, *Progress in Photovoltaics: Research and Applications,* Vol. 19, Issue 7, 2011, pp. 894-897.

[3]. A. Nozik, Quantum dot solar cells, *Physica E: Low-dimensional Systems and Nanostructures*, Vol. 14, Issue 1-2, 2002, pp. 115-120.

[4]. B. Oregan, M. Gratzel, A Low-cost, High-efficiency Solar Cell Based on Dye-sensitized Colloidal TiO_2 Films, *Nature*, Vol. 353, No. 6346, 1991, pp. 737-740.

[5]. G. Yu, J. Gao, J. C. Hummelen, F. Wudl, A. J. Heeger, Polymer Photovoltaic Cells: Enhanced Efficiencies via a Network of Internal Donor-Acceptor Heterojunctions, *Science*, Vol. 270, Issue 5243, 1995, pp. 1789-1791.

[6]. M. M. Lee, J. Teuscher, T. Miyasaka, T. N. Murakami, H. J. Snaith, Efficient hybrid solar cells based on meso-superstructured organometal halide perovskites, *Science*, Vol. 338, Issue 6107, 2012, pp. 643-647.

[7]. W. Zhang, M. Saliba, S. D. Stranks, Y. Sun, X. Shi, U. Wiesner, H. J. Snaith, Enhancement of Perovskite-Based Solar Cells Employing Core–Shell Metal Nanoparticles, *Nano Letters*, Vol. 13, Issue 9, 2013, pp. 4505-4510.

[8]. A. Kojima, M. Ikegami, K. Teshima, T. Miyasaka, Highly Luminescent Lead Bromide Perovskite Nanoparticles Synthesized with Porous Alumina Media, *Chemistry Letters*, Vol. 41, Issue 4, 2012, pp. 397-399.

[9]. C. R. Kagan, D. B. Mitzi, C. D. Dimitrakopoulos, Organic-Inorganic Hybrid Materials as Semiconducting Channels in Thin-Film Field-Effect Transistors, *Science*, Vol. 286, Issue 5441, 1999, pp. 945-947.

[10]. A. Kojima, K. Teshima, Y. Shirai, T. Miyasaka, Organometal Halide Perovskites as Visible-Light Sensitizers for Photovoltaic Cells, *Journal of the American Chemical Society,* Vol. 131, Issue 17, 2009, pp. 6050-6051.

[11]. J. Burschka, N. Pellet, S. J. Moon, R. Humphry-Baker, P. Gao, M. K. Nazeeruddin, M. Grätzel, Sequential deposition as a route to high-performance perovskite-sensitized solar cells, *Nature*, Vol. 499, 2013, pp. 316-319.

[12]. J. H. Heo, S. H. Im, J. H. Noh, T. N. Mandal, C. Lim, J. A. Chang, Y. H. Lee, H. Kim, A. Sarkar, M. K. Nazeeruddin, M. Grätzel, S. I. Seok, Efficient inorganic–organic hybrid heterojunction solar cells containing perovskite compound and polymeric hole conductors, *Nature Photonics*, Vol. 7, 2013, pp. 486-491.

[13]. J. H. Noh, S. H. Im, J. H. Heo, T. N. Mandal, S. I. Seok, Chemical Management for Colorful, Efficient, and Stable Inorganic–Organic Hybrid Nanostructured Solar Cells, *Nano Letters*, Vol. 13, Issue 4, 2013, pp. 1764-1769.

[14]. H. S. Kim, C. R. Lee, J. H. Im, K. B. Lee, T. Moehl, A. Marchioro, S. J. Moon, R. Humphry-Baker, J. H. Yum, J. E. Moser, M. Grätzel, N. G. Park, Lead iodide perovskite sensitized all-solid-state submicron thin film mesoscopic solar cell with efficiency exceeding 9 %, *Scientific Reports*, Vol. 2, 2012, pp. 1-7.

[15]. V. Thavasi, V. Renugopalakrishnan, R. Jose, S. Ramakrishna, Controlled electron injection and transport at materials interfaces in dye sensitized solar cells, *Materials Science and Engineering: R Reports*, Vol. 63, Issue 3, 2009, pp. 81-99.

[16]. B. S. Ong, C. S. Li, Y. N. Li, Y. L. Wu, R. Loutfy, Stable, Solution-Processed, High-Mobility ZnO Thin-Film Transistors, *Journal of the American Chemical Society*, Vol. 129, Issue 10, 2007, pp. 2750-2751.

[17]. C. Lee, X. Wei, J. W. Kysar, J. Hone, Measurement of the Elastic Properties and Intrinsic Strength of Monolayer Graphene, *Science*, Vol. 321, Issue 5887, 2008, pp. 385-388.

[18]. S. Chen, Q. Wu, C. Mishra, J. Kang, H. Zhang, K. Cho, W. Cai, A. A. Balandin, R. S. Ruoff, Thermal conductivity of isotopically modified graphene, *Nature Materials*, Vol. 11, No. 3, 2012, pp. 203-207.

[19]. A. A. Balandin, S. Ghosh, W. Bao, I. Calizo, D. Teweldebrhan, F. Miao, C. N. Lau, Superior Thermal Conductivity of Single-Layer Graphene, *Nano Letters*, Vol. 8, Issue 3, 2008, pp. 902-907.

[20]. J. H. Chen, C. Jang, S. Xiao, M. Ishigami, M. S. Fuhrer, Intrinsic and extrinsic performance limits of graphene devices on SiO_2, *Nature Nanotechnology*, Vol. 3, 2008, pp. 206-209.

[21]. A. K. Geim, K. S. Novoselov, The rise of graphene, *Nature Materials*, Vol. 6, No. 3, 2007, pp. 183-191.

[22]. Q. Y. He, S. X. Wu, Z. Y. Yin, H. Zhang, Graphene-based electronic sensors, *Chemical Science*, Vol. 3, 2012, pp. 1764-1772.
[23]. X. Huang, Z. Zeng, Z. Fan, J. Liu, H. Zhang, Graphene-Based Electrodes. *Advanced Materials*, Vol. 24, Issue 45, 2012, pp. 5979-6004.
[24]. Z. Yin, J. Zhu, Q. He, X. Cao, C. Tan, H. Chen, Q. Yan, H. Zhang, Graphene-Based Materials for Solar Cell Applications, *Advanced Energy Materials,* Vol. 4, Issue 1, 2014, pp. 1-9.
[25]. Y. Zhang, Z. R. Tang, X. Fu, Y. J. Xu, Engineering the Unique 2D Mat of Graphene to Achieve Graphene-TiO_2 Nanocomposite for Photocatalytic Selective Transformation: What Advantage does Graphene Have over Its Forebear Carbon Nanotube?, *ACS Nano*, Vol. 5, Issue 9, 2011, pp. 7426-7435.
[26]. C. Zhu, S. Guo, P. Wang, L. Xing, Y. Fang, Y. Zhai, S. Dong, One-pot, water-phase approach to high-quality graphene/TiO_2 composite nanosheets, *Chemical Communications*, Vol. 46, No. 38, 2010, pp. 7148-7150.
[27]. Y. Liang, H. Wang, H. S. Casalongue, Z. Chen, H. Dai, TiO_2 Nanocrystals Grown on Graphene as Advanced Photocatalytic Hybrid Materials, *Nano Research*, Vol. 3, Issue 10, 2010, pp. 701-705.
[28]. W. S. Hummers, R. E. Offeman, Preparation of Graphitic Oxide, *Journal of the American Chemical Society*, Vol. 80, Issue 6, 1958, pp. 1339.
[29]. D. H. Wang, D. W. Choi, J. Li, Z. G. Yang, Z. M. Nie, R. Kou, D. H. Hu, C. M. Wang, L. V. Saraf, J. G. Zhang, Self-Assembled TiO_2-Graphene Hybrid Nanostructures for Enhanced Li-Ion Insertion, *ACS Nano*, Vol. 3, Issue 4, 2009, pp. 907-914.
[30]. L. Etgar, P. Gao, Z. Xue, Q. Peng, A. K. Chandiran, B. Liu, M. K. Nazeeruddin, M. Grätzel, Mesoscopic $CH_3NH_3PbI_3/TiO_2$ Heterojunction Solar Cells, *Journal of the American Chemical Society*, Vol. 134, Issue 42, 2012, pp. 17396-17399.
[31]. K. Dai, L. Lu, Q. Liu, G. Zhu, Q. Liua, Z. Liua, Graphene oxide capturing surface-fluorinated TiO_2 nanosheets for advanced photocatalysis and the reveal of synergism reinforce mechanism, *Dalton Transactions*, Vol. 43, Issue 5, 2014, pp. 2202-2210.
[32]. Y. W. Jun, M. F. Casula, J. H. Sim, S. Y. Kim, J. Cheon, A. P. Alivisatos, Surfactant-Assisted Elimination of a High Energy Facet as a Means of Controlling the Shapes of TiO_2 Nanocrystals, *Journal of the American Chemical Society*, Vol. 125, Issue 51, 2003, pp. 15981-15985.
[33]. P. G. Liu, K. C. Gong, P. Xiao, M. Xiao, Preparation and characterization of poly(vinyl acetate)-intercalated graphite oxide nanocomposites, *Journal of Materials Chemistry*, Vol. 10, No. 4, 2000, pp. 933-935.
[34]. Y. W. Jun, M. F. Casula, J. H. Sim, S. Y. Kim, J. Cheon, A. P. Alivisatos, Surfactant-Assisted Elimination of a High Energy Facet as a Means of Controlling the Shapes of TiO_2 Nanocrystals, *Journal of the American Chemical Society,* Vol. 125, Issue 51, 2003, pp. 15981-15985.
[35]. J. Lu, J. X. Yang, J. Wang, A. Lim, S. Wang, K. P. Loh, One-pot synthesis of fluorescent carbon nanoribbons, nanoparticles, and graphene by the exfoliation of graphite in ionic liquids, *ACS Nano*, Vol. 3, Issue 8, 2009, pp. 2367-2375.
[36]. A. C. Ferrari, J. C. Meyer, V. Scardaci, C. Casiraghi, M. Lazzeri, F. Mauri, S. Piscanec, D. Jiang, K. S. Novoselov, S. Roth, A. K. Geim, Raman Spectrum of Graphene and Graphene Layers, *Physical Review Letters*, Vol. 97, No. 18, 2006, pp. 187401-187404.
[37]. M. A. Pimenta, G. Dresselhaus, M. S. Dresselhaus, L. A. Cancado, A. Jorio, R. Saito, Studying disorder in graphite-based systems by Raman spectroscopy, *Physical Chemistry Chemical Physics*, Vol. 9, 2007, pp. 1276-1290.
[38]. A. C. Ferrari, Raman spectroscopy of graphene and graphite: Disorder, electron–phonon coupling, doping and nonadiabatic effects, *Solid State Communications*, Vol. 143, 2007, pp. 47-57.
[39]. Y. Lei, L. D. Zhang, J. C. Fan, Fabrication, characterization and Raman study of TiO_2 nanowire arrays prepared by anodic oxidative hydrolysis of $TiCl_3$, *Chemical Physics Letters*, Vol. 338, Issue 4-6, 2001, pp. 231-236.
[40]. L. L. Zhang, S. Zhao, X. N. Tian, X. S. Zhao, Layered Graphene Oxide Nanostructures with Sandwiched Conducting Polymers as Supercapacitor Electrodes, *Langmuir*, Vol. 26, Issue 22, 2010, pp. 17624-17628.
[41]. G. Wang, J. Yang, J. Park, X. Gou, B. Wang, H. Liu, J. Yao, Facile Synthesis and Characterization of Graphene Nanosheets, *The Journal of Physical Chemistry C,* Vol. 112, Issue 22, 2008, pp. 8192-8195.